Int. J. Heat Mass Transfer. Vol. 24, No. 10, pp. 1681–1698, 1981
Printed in Great Britain

0017 9310/81/101681 18 $02.00/0

COMBINED RADIATION AND CONVECTION IN ABSORBING, EMITTING AND ANISOTROPICALLY SCATTERING GAS–PARTICULATE TUBE FLOW

F. H. AZAD
Dept. of Mechanical Engineering, Aeronautical Engineering & Mechanics, Rensselaer Polytechnic Institute, Troy, N.Y.

and

M. F. MODEST
Dept. of Mechanical Engineering, University of Southern California, Los Angeles, California

(*Received* 9 *February* 1981 *and in revised form* 16 *April* 1981)

Abstract—A numerical procedure has been developed to investigate the interaction of thermal radiation with conduction and convection in thermally developing gas–particulate suspension flow through a circular tube. In the present study an analysis is performed on the turbulent flow of a multiphase medium with absorbing, emitting and anisotropically scattering particulates bounded by a heated or cooled constant-temperature wall. The contribution of thermal radiation is obtained by modification of the differential approximation to accommodate linear-anisotropic scattering, which is shown to be accurate by comparison with some exact solutions. The governing differential equations are derived as three coupled (non-linear) equations which are solved numerically by an implicit finite difference method with iterative procedure of the particulate terms. The results are summarized for wide ranges of parameters.

NOMENCLATURE

A_p, surface area of single particle $= \pi d_p^2$;
a_1, degree of anisotropy, $-1 \le a_1 \le +1$
C, specific heat at constant pressure;
C_1, dimensionless particle to gas film coefficient;
C_2, specific mass loading ratio;
D, pipe diameter;
d_p, particle diameter;
f, fanning friction factor;
f_1, dimensionless fluid velocity function, $\rho_f u_f / 2\rho_f \bar{u}_f$;
f_2, dimensionless fluid diffusivity function, $(1+\varepsilon_M Pr/\nu)$;
f_4, f_5, dimensionless radial variables;
g_1, dimensionless axial variable;
h, heat-transfer coefficient for pipe flow;
h_p, heat-transfer coefficient for flow over solid particle;
k_f, thermal conductivity of fluid;
kR_t, dimensionless turbulent Reynolds number;
M_R, dimensionless conduction–radiation parameter, $k_f/4\sigma T_i^3 R$;
Nu_x, local Nusselt number;
n_p, number of solid particles per unit volume;
Pr, Prandtl number, $\mu_f C_f / k_f$;
p_1, dimensionless particle velocity function, $n_p V_p \rho_p u_p / 2 n_p V_p \rho_p \bar{u}_p$;
q, heat flux;
q, dimensionless heat flux, $qR/k_f T_i$;
R, pipe radius;
Re_D, gas Reynolds number $\bar{u}_f D/\nu$;
r, radial distance;
T, temperature;
u, axial velocity;
$\bar{u}$, average or bulk velocity;
V_p, solid particle volume;
x, axial coordinate;
y^+, z, dimensionless radial coordinates;
ε, eddy diffusivity, wall emissivity;
η, dimensionless radial coordinate, r/R;
κR, optical thickness based on absorption;
θ, dimensionless temperature;
$\Delta\theta_p$, dimensionless temperature difference, $\theta_p - \theta_f$;
μ, dynamic viscosity;
ν, kinematic viscosity;
ρ, density;
σ, Stefan–Boltzmann constant;
τ_o, total optical thickness, $\kappa R/(1-\omega)$;
ψ, dimensionless axial coordinate;
ω, single scattering albedo, $0 \le \omega \le 1$.

Subscripts

f, fluid;
H, heat;
i, inlet;
M, momentum;
m, single-phase mean;
mm, suspension mixed mean;
p, particle;
w, wall.

Superscripts

$+$,	dimensionless turbulent quality;
C,	convective;
R,	radiative;
T,	Total.

INTRODUCTION

THERE is a large variety of industrial applications in which the heat transfer rates in flowing mixtures of gases and solid or liquid particles are of importance. These applications range from waste heat extraction from flue gases, nuclear reactor cooling (steam–droplet mixtures), and solid-propellant rockets (product gases and metallic particles used to increase the thermal conductivity of the propellant resulting in hgher thrusts), to MHD generators (product gases seeded to improve electrical conductivity). Probably the most important applications of gas–particulate mixtures today are in the area of combustion of fuel for power production (oil burning, pulverised-coal combustion and, in the near future, combustion of coal in fluidized beds).

The increase of heat transfer rates is a prominent characteristic in multiphase suspensions. The particles influence heat transfer rates by disturbing the laminar or turbulent flow structure. This occurs in several ways: (i) penetration of solids through the buffer layer and into the laminar sublayer causes a thinning of the viscous sublayer and a reduction in the resistance to convective heat transfer; (ii) the presence of solids may cause a damping of the convective eddies and adversely affect the turbulent transport of energy; and (iii) energy exchange between the laminar sublayer and turbulent core is promoted by the radial motion of the particulates. Furthermore, the high volumetric heat capacity of the solid compared with that of the fluid prolongs the thermal entry length and increases the two-phase heat transfer. In addition to the above phenomena, in high-temperature applications the interaction of radiant energy with the participating medium is of importance. This interaction can profoundly increase the overall heat transfer rate due to the large absorptivity of the cloud of fine particles.

Experiments by Farbar and Morley [1] first demonstrated that it was possible to increase heat transfer rates by adding solid particles to gas flow. The first analytical treatment made on heat transfer in a turbulent suspension has been published by Tien [2], who predicted higher heat transfer rates for the thermal entry length. Comparison of experiments by Farbar and Depew [3, 4] with theory [2] demonstrated that even in the absence of high-temperature effects the convection in gas–particulate suspensions is not well understood. However, experiment [3, 4] also shows that, at moderate temperatures, the heat transfer is only moderately increased unless the particle mass loading ratio becomes very large. Echigo *et al.* [5, 6] and Tamehiro *et al.* [7] have performed numerical analyses on the heat transfer with fully developed laminar and turbulent flow of gaseous suspensions with radiatively absorbing and emitting particulates between parallel plates and in circular tubes. The only work considering combined convection radiation with scattering appears to be the one by Chawla and Chan [8]. However, their study is limited to laminar flow between parallel plates with isotropic scattering. To date, no analysis has been performed to include the important effects of anisotropic radiative scattering in gas–particulate suspensions.

It is the purpose of this paper to investigate the combined convective and radiative effects in turbulent tube flow of an absorbing, emitting and linear anisotropically scattering gas–particulate suspension. The governing differential equations are derived as three coupled (non-linear) equations, which are solved numerically by an implicit finite difference method with iterative procedure of the particulate terms. The contribution of thermal radiation is obtained by modification of the differential approximation to accommodate linear–anisotropic scattering. Results are reported as a parametric study of the interaction of predominant convective and radiative parameters and their effects on the Nusselt number, mixed-mean temperature and radiative flux.

ANALYSIS

Assumptions

In the present investigation the following major simplifying assumptions are made:

1. The pipe wall is isothermal (T_w = const) and gray.
2. The flow field of the two phases is hydrodynamically fully developed and has a laminar or turbulent velocity distribution. The temperatures of the particles and the gas are equal and constant at the inlet.
3. The fluid and particle properties are temperature independent.
4. The particles are spheres of uniform size and their thermal conductivity is large enough to neglect radial variation of temperature within the sphere (small Biot number).
5. The particles are uniformly distributed throughout the pipe cross-section and are sufficiently small and numerous to be considered as a continuum.
6. The time–mean velocities of the two phases are equal and the presence of the particles has no effect on the velocity profile, eddy diffusivities for heat or momentum, or the friction factor of the gas.
7. The eddy diffusivity of the particles is negligible.
8. The energy transport by collisions among particles or with the wall are negligible.
9. Viscous dissipation is not included.
10. The solids are gray absorbing, emitting and linear–anisotropically scattering particu-

lates; the gas is transparent to radiation.

11. The radiative transfer in the axial direction is neglected as compared with the radial heat transfer; this has been shown to be a good approximation except for regions close to a temperature jump [9].

Some of the above assumptions are not necessarily very good. For example, assumptions (5), (6), and (7) are made primarily because at present no theory or experimental correlations exist to predict the influence of these effects. However, if strong radiation is present the introduced inaccuracies become less and less important. A number of the above assumptions are invoked only in the presentation of parametric results, i.e. the theory developed below is not limited by assumptions (1), (3), (5), (6), and (7). Of course, if assumption (3) is to be relaxed, no hydrodynamically fully developed velocity profile exists, and simultaneous solution of the momentum equation becomes necessary. However, in the light of the uncertainties present in the evaluation of gas–particulate interaction, it may be sufficient to assume negligible radial velocities, reducing the continuity equation to $\rho u = \rho u(r)$ only. In the following analysis, assumption (3) is relaxed in this fashion, while for the presentation of results only temperature-independent properties will be employed.

Basic equations

Based on the foregoing postulations an energy balance in the cylindrical coodinate system (see Fig. 1) yields the basic equations governing the temperature field. For the gas phase

$$\rho_f C_f u_f \frac{\partial T_f}{\partial x} = n_p h_p A_p (T_p - T_f) + \frac{1}{r}\frac{\partial}{\partial r}\left[r(k_f + \rho_f C_f \varepsilon_{H,f})\frac{\partial T_f}{\partial r}\right], \quad (1)$$

and for the particulates,

$$n_p V_p \rho_p C_p u_p \frac{\partial T_p}{\partial x} = n_p h_p A_p (T_f - T_p) + \frac{1}{r}\frac{\partial}{\partial r}\left[r n_p V_p \rho_p C_p \varepsilon_{H,p}\frac{\partial T_p}{\partial r}\right] - \frac{1}{r}\frac{\mathrm{d}}{\mathrm{d}r}(rq^R), \quad (2)$$

subject to the boundary conditions

$$r = 0: \frac{\partial T_f}{\partial r} = 0;\ x = 0:\ T_f = T_p = T_{in},$$
$$r = R:\ T_f = T_w. \quad (3)$$

These equations are essentially the same as the ones of Tien [2], with the exception that the present formulation allows the incorporation of a more sophisticated radiation model, similar to that of Tamehiro *et al.* [7]. Note that there may be a temperature discontinuity between the wall and the particles at the wall, due to the absence of a conduction term in equation (2). In the absence of thermal radiation there would be no temperature slip, due to assumption (6). If radiation is important, the temperature slip can be evaluated from equation (2) as

$$n_p h_p A_p (T_w - T_p)|_{r=R} = \frac{1}{r}\frac{\partial}{\partial r}(rq^R)|_{r=R}. \quad (4)$$

The exact equations for the radiative heat flux in 1-D, gray, linear-anisotropically scattering media have been derived by Azad and Modest [10]. There are two reasons for limiting the discussion to linear-anisotropic scattering: (1) Exact analytical solutions are practically impossible to obtain for higher-order scattering phase functions. This is due to the fact that the azimuthal direction cannot be eliminated by integration as in the planar case, resulting in higher-order integral equations in the radial and local direction coordinates. (2) The accuracy of a linear-anisotropic approximation to realistic scattering phase functions in heat transfer applications without collimated irradiation was established in a previous paper [12]. There any forward-scattering peak was removed from the phase function and treated as transmitted. Backward-scattering peaks were removed in a similar fashion, while the remnant of the scattering phase function was approximated by

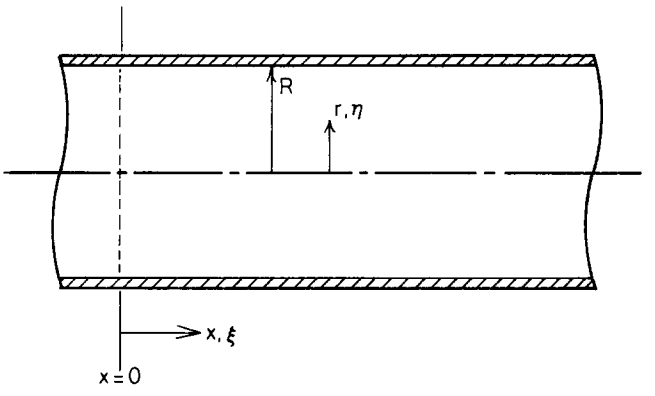

FIG. 1. Coordinate systems.

linear–anisotropic scattering. Using the resulting modified scattering coefficient and modified phase function gave excellent prediction of radiative transfer rates as long as the phase function was relatively smooth and had insignificant back-scattering.

Incorporation of the exact integral formulation for linear–anisotropic scattering would lead to excessive computer time demands in the present flow problems. However, they also showed that their modified differential approximation [11, 12] yields results to within a few percent accuracy for any realistic temperature profile. Thus this model is used here as well as the results in [10], *viz.*

$$\frac{1}{r}\frac{\partial}{\partial r}\left(r\frac{\partial q^R}{\partial r}\right)-\left[\frac{3\kappa^2}{1-\omega}\left(1-\frac{a_1\omega}{3}\right)+\frac{1}{r^2}\right]q^R = 4\sigma\kappa\frac{\partial T_p^4}{\partial r}, \quad (5)$$

subject to the boundary conditions

$$r=0:\ q^R=0; \quad (6)$$

$$r=R:\ \frac{\mathrm{d}q^R}{\mathrm{d}r}+\left[\frac{1}{R}+2\left(\frac{2-\varepsilon}{\varepsilon}\right)\kappa\right]q^R = 4\sigma\kappa[T_p^4-T_w^4],$$

where ε is the emissivity of the wall.

In equation (5) a_1 represents the degree of anisotropy, where $-1\le a_1\le+1$. For $a_1>0$ forward scattering dominates, while $a_1<0$ results in mostly backward scattering. In the present case of a two-phase flow with radiatively participating particulates through a circular tube, equations (1), (2), and (5) are the governing equations of the system with T_f, T_p and q^R to be determined.

The 3-layer turbulent velocity distribution for fully developed flow, presented in Kays [13] for the laminar sublayers, and as proposed by Reichardt [14] for the turbulent core, are used and given by:

laminar sublayer:

$$u^+ = y^+,\quad 0<y^+<5;$$

buffer layer:

$$u^+ = -3.05+5.0\ln y^+,\ 5\le y^+<30; \quad (7)$$

Turbulent core:

$$u^+ = 5.5+2.5\ln\left[y^+\frac{1.5(1+r/R)}{1+2(r/R)^2}\right],\quad y^+>30.$$

The momentum eddy viscosity for the gas, ε_M, is described by the 2-layer model. The wall region ($y^+<40$), as described by the Van Driest model modified by Spalding [15], results in

$$\frac{\varepsilon_M}{\nu}=\frac{k}{E}\left[\mathrm{e}^{ku^+}-1-ku^+-\frac{(ku^+)}{2!}-\frac{(ku^+)^3}{3!}\right],\ y^+<40, \quad (8a)$$

where $k=0.407$ and $E=10$.

In the turbulent core the Reichardt model [14]

$$\frac{\varepsilon_M}{\nu}=\frac{kR^+}{6}[1-(r/R)^2][1+2(r/R)^2],\ y^+\ge40 \quad (8b)$$

is employed. In the above equations the standard non-dimensional quantities

$$u^+=\frac{u}{2\bar{u}\sqrt{(f/8)}},\ y^+=\frac{y}{R}\mathrm{Re}\sqrt{(f/8)},\ R^+=\mathrm{Re}\sqrt{(f/8)} \quad (9)$$

have been introduced.

The eddy diffusivity for heat, ε_H, is calculated using the standard assumption that the turbulent Prandtl number is approximately equal to unity, i.e. $Pr_t=\varepsilon_M/\varepsilon_H\simeq1$.

The definition of a mixed-mean temperature and, therefore, of a Nusselt number presents some problem if the specific heats of gas and particulates are temperature-dependent. Fortunately, strong temperature dependence of specific heats is rare, and it is assumed here that it may be approximated by

$$C_f=C_{fi}\left(\frac{T_f}{T_i}\right)^{n_f},\quad C_p=C_{pi}\left(\frac{T_p}{T_i}\right)^{n_p}. \quad (10)$$

Now defining an overall mixture mixed-mean temperature in terms of enthalpies as

$$\dot{m}_f h_{fm}+\dot{m}_p h_{pm}=\dot{m}_f h_{fmm}+\dot{m}_p h_{pmm}, \quad (11)$$

where

$$h_{fm}=\frac{2}{\rho_f u_f R^2}\int_0^R \rho_f u_f h_f r\,\mathrm{d}r, \quad (12)$$

$$h_{pm}=\frac{2}{n_p V_p \rho_p u_p R^2}\int_0^R n_p V_p \rho_p u_p h_p r\,\mathrm{d}r, \quad (13)$$

leads to

$$T_{fm}=\frac{2}{\rho_f u_f C_{fm} R^2}\int_0^R \rho_f u_f C_f T_f r\,\mathrm{d}r, \quad (14)$$

$$T_{pm}=\frac{2}{n_p V_p \rho_p u_p C_{pm} R^2}\int_0^R n_p V_p \rho_p u_p C_p T_p r\,\mathrm{d}r \quad (15)$$

$$T_{mm}=\frac{(1+n_p)\dot{m}_f C_{fm} T_{fm}+(1+n_f)\dot{m}_p C_{pm} T_{pm}}{(1+n_p)\dot{m}_f C_{fmm}+(1+n_f)\dot{m}_p C_{pmm}}. \quad (16)$$

The mixture mixed-mean temperature can also be evaluated through axial integration from

$$T_{mm}=T_i-2\pi R\int_0^x \frac{q^T\mathrm{d}x}{\dot{m}_f C_{fmm}+\dot{m}_p C_{mm}}, \quad (17)$$

where q^T is the total heat flux (convective and radiative) at the tube wall, i.e.

$$q^T=q^C+q^R, \quad (18)$$

where the convective flux is evaluated from

$$q^C=-k_f\left.\frac{\partial T_f}{\partial r}\right|_{r=R}, \quad (19)$$

and the radiative flux, q^R, is found from equation (6).

The Nusselt number for the gas–particulate suspension is defined as

$$Nu_x \equiv \frac{2hR}{k_f} = \frac{2q^T R}{k_f(T_{mm} - T_w)}. \tag{20}$$

If radial integration for T_{mm} is used, equation (16), Nu_x is evaluated from

$$Nu_x = \frac{2R}{T_w - T_{mm}}\left[\frac{\partial T_f}{\partial r} - \frac{q^R}{k_f}\right]_{r=R} \tag{21}$$

For axial integration, equation (17), on the other hand, Nu_x is determined from

$$Nu_x = \frac{1}{\pi k_f}(\dot{m}_f C_{fmm} + \dot{m}_p C_{pmm})\frac{1}{T_w - T_{mm}}\frac{dT_{mm}}{dx}. \tag{22}$$

The governing equations may be non-dimensionalized by introducing the following quantities:

$$\theta_f = \frac{T_f}{T_i};\ \theta_p = \frac{T_p}{T_i};\ \Delta\theta_p = \theta_p - \theta_f,$$

$$\bar{q} = \frac{qR}{k_{fi}T_i};\ \eta = \frac{r}{R};\ \bar{x} = \frac{x}{R};$$

$$C_1 = \left(\frac{R}{d_p}\right)^2 d_p n_p Nu_p A_p;\ Nu_p = \frac{h_p d_p}{k_{fi}};$$

$$C_2 = \frac{\dot{m}_p}{\dot{m}_f} = \frac{\overline{n_p V_p \rho_p u_p}}{\overline{\rho_f u_f}}; \tag{23}$$

$$Re_i = \frac{2\overline{\rho_f u_f} R}{\mu_{fi}};\ Pr_i = \frac{\mu_{fi} C_{fi}}{k_{fi}};\ M_R = \frac{k_{fi}}{4\sigma T_i^3 R};$$

$$f_1 = \frac{1}{2}\frac{\rho_f u_f}{\overline{\rho_f u_f}};\ f_2 = \frac{k_f}{k_{fi}}\left(1 + \frac{\varepsilon_{M,f}}{\nu}\frac{Pr}{Pr_t}\right);\ f_3 = \frac{C_f}{C_{fi}};$$

$$p_1 = \frac{1}{2}\frac{n_p V_p \rho_p u_p}{\overline{n_p V_p \rho_p u_p}};\ p_2 = \frac{n_p V_p \rho_p C_p \varepsilon_{H,p}}{k_{fi}};\ p_3 = \frac{C_p}{C_{fi}}.$$

This leads to

$$f_1 f_3 Re_i Pr_i \frac{\partial\theta_f}{\partial\bar{x}} = C_1(\theta_p - \theta_f) + \frac{1}{\eta}\frac{\partial}{\partial\eta}\left[\eta f_2 \frac{\partial\theta_f}{\partial\eta}\right], \tag{24}$$

$$p_1 p_3 C_2 Re_i Pr_i \frac{\partial\theta_p}{\partial\bar{x}} = C_1(\theta_f - \theta_p) + \frac{1}{\eta}\frac{\partial}{\partial\eta}\left[\eta p_2 \frac{\partial\theta_p}{\partial\eta}\right] - \frac{1}{\eta}\frac{d}{d\eta}(\eta\bar{q}^R), \tag{25}$$

$$\frac{1}{\eta}\frac{d}{d\eta}\left(\eta\frac{d\bar{q}^R}{d\eta}\right) - \left[\frac{3(\kappa R)^2}{1-\omega}\left(1 - \frac{a_1\omega}{3}\right) + \frac{1}{\eta^2}\right]\bar{q}^R = \frac{\kappa R}{M_R}\frac{\partial\theta_p^4}{\partial\eta}, \tag{26}$$

$$\bar{x} = 0;\ \theta_f = \theta_p = 1;$$

$$\eta = 0;\ \frac{\partial\theta_f}{\partial\eta} = 0;\ \bar{q}^R = 0; \tag{27}$$

$$\eta = 1:\ \theta_f = \theta_w;$$

$$\frac{1}{\eta}\frac{d}{d\eta}(\eta\bar{q}^R) + 2\left(\frac{2}{\varepsilon} - 1\right)\kappa R\bar{q}^R = \frac{\kappa R}{M_R}[\theta_p^4 - \theta_w^4].$$

For stability of numerical calculations, equations (24) and (25) are further transformed by using

$$z = \ln[kR_t(1-\eta)+1];\ \psi = \ln[C\bar{x}+1],$$

$$f_4 = (kR_t e^{-z})^2;\ f_5 = (kR_t+1)/(kR_t+1-e^z), \tag{28}$$

$$kR_t = 0.4\sqrt{(f/8)}\,Re_i;\ g_1 = Ce^{-\psi}\,Re_i\,Pr_i,$$

where z is a stretched radial coordinate which places a lot of nodes near the wall, and ψ is a stretched axial coordinate, which places a lot of nodes near the inlet, depending on the choice for the constant C. Thus:

$$f_1 f_3 g_1 \frac{\partial\theta_f}{\partial\psi} = -f_2 f_5 f_4 \frac{\partial\theta_f}{\partial z} + f_4\frac{\partial}{\partial z}\left\{f_2\frac{\partial\theta_f}{\partial z}\right\} + C_1\Delta\theta_p, \tag{29}$$

$$p_1 p_3 C_2 g_1 \frac{\partial\theta_p}{\partial\psi} = -p_2 f_5 f_4 \frac{\partial\theta_p}{\partial z} + f_4\frac{\partial}{\partial z}\left\{p_2\frac{\partial\theta_p}{\partial z}\right\} - C_1\Delta\theta_p - \frac{1}{\eta}\frac{\partial}{\partial\eta}(\eta\bar{q}^R). \tag{30}$$

The values for $\Delta\theta_p = \theta_p - \theta_f$ are usually very small as compared to θ_f (combined with $C_1 \gg 1$). In fact, for small particles without chemical reactions (such as combustion), θ_f and θ_p are often so close that usage of a single energy equation would be adequate. Therefore, in actual numerical calculations the particle energy equation (30) is replaced by one based on $\Delta\theta_p$. This is achieved by multiplying equation (29) by $p_1 p_3 C_2/f_1 f_3$ and subtracting it from equation (30).

For the calculations of the radiative flux equally-spaced nodes result in better numerical stability. Therefore, equation (26) is not transformed with respect to z. Rather, values of q^R and θ_p are passed back and forth between equations (26) and (30) by the use of splines.

Using the non-dimensionalization and transformations, the expressions for mixed-mean temperatures become:

$$f_{3m}\theta_{fm} = \frac{4}{kR_t}\int_0^{\ln(kR_t+1)} f_1 f_3 \theta_f \eta e^z dz, \tag{31}$$

$$p_{3m}\theta_{pm} = \frac{4}{kR_t}\int_0^{\ln(kR_t+1)} p_1 p_3 \theta_p \eta e^z dz, \tag{32}$$

and

$$\theta_{mm} = \frac{(1+n_p)f_{3m}\theta_{fm} + (1+n_f)p_{3m}C_2\theta_{pm}}{(1+n_p)f_{3mm} + (1+n_f)p_{3mm}C_2} \quad \text{(radial integration)}, \tag{33}$$

or

$$\theta_{mm} = 1 - 4\int_0^{\psi}\frac{\bar{q}^T}{f_{3mm} + C_2 p_{3mm}}\frac{d\psi}{g_1} \quad \text{(axial integration)}. \tag{34}$$

Finally, the Nusselt number is evaluated from

$$Nu = \frac{2}{\theta_{mm} - \theta_w}\left[kR_t \left.\frac{\partial \theta_f}{\partial z}\right|_{z=0} + \frac{\bar{q}_w^R}{f_{2w}}\right]$$

(radial integration), (35)

$$Nu = \frac{g_1}{2f_{2w}} \frac{f_{3mm} + C_2 p_{3mm}}{\theta_w - \theta_{mm}} \frac{d\theta_{mm}}{d\psi}$$

(axial integration). (36)

Comparison between results from radial and axial integration schemes was used to check numerical stability and served as a criterion to establish the optimum number of radial nodes and axial stepping.

RESULTS AND DISCUSSION

Temperature profile

For completeness, the general trends of the gas–particulate temperature profiles will be discussed briefly before examining the heat transfer results. If one neglects radiation (low temperature cases) for a flow of a cold mixture through a hot tube ($T_w/T_i > 1$), heat transfer takes place as follows: The carrier gas gains heat by convection from the tube walls, while the particles gain heat from the gas due to the forming temperature difference. Thus the heat-up of the particles lags behind that of the gas. However, if substantial particle radiation is present (higher temperature cases), this is not necessarily the case, due to direct energy exchange between hot wall and cold particles. Results show that the temperature of the particles is higher than that of the gas in the central core while in the proximity of the wall it is lower than that of the gas with the intersection of both temperature profiles moving toward the wall with decreasing M_R, and increasing x/R. Similarly, the opposite is true if $T_w/T_i < 1$.

Heat transfer results

To establish the accuracy of the numerical code the predicted convective Nusselt numbers based on the mixed-mean temperature were compared with analytical results for laminar and turbulent pipe flow for a transparent gas (no particles) for $Pr = 1$. For laminar flow the computed Nu was found to be within 0.3% of the theoretical Nusselt number for all values of $(x/R)/Re.Pr > 10^{-5}$. For turbulent flow the radially computed asymptotic Nusselt number, Nu_x, is within 5% (high side for all Re_D) of the modified Dittus–Boelter formula $Nu_x = 0.021\, Re_D^{0.8}\, Pr^{0.33}$ for $5000 < Re_D < 100{,}000$ (T_w = constant). Numerical computing of Nusselt numbers within a few percent of experimental results is a common problem for turbulent flow because of the diffusivity schemes employed. Thus various refinements in eddy diffusivity models are normally included, such as those presented in Kays [13], by modification of the diffusivity ratio of heat and momentum to bring the final results into close correspondence with experimental data. However, an error within +5% of the empirical formula for all turbulent Reynolds numbers investigated is certainly within the required accuracy of most engineering applications. Further verification of the code's accuracy was established by running gas particulate flows with varying mass-loading ratios. The code accuracy and numerical results remained unchanged from the gas-only case except for a shifting in the x-coordinate by a factor equal to the equivalent specific mass loading ratio $(1 + C_2)$, as predicted by Tien [2].

The accuracy of the differential approximation as a reliable radiation model was established by Azad and Modest [11, 12]. In order to ascertain that errors from the differential approximation would not accumulate when applied to a long pipe, some test-runs were made also using the exact integral formulation from [10] for the radiative flux in equation (30). Figure 2 shows a comparison between the mixed-mean temperatures for various combinations of total optical thickness, $\tau_0 = \kappa R/(1-\omega)$, and the conduction–radiation parameter, M_R. The two results are in excellent agreement and the dominant trend shown is that the mixed-mean temperatures predicted by the exact solution lag behind those obtained from the differential approximation. The reason for this behavior is characteristic of the differential approximation which always overpredicts the radiative heat flux at the tube wall. Figure 3 depicts the corresponding comparison between the Nusselt numbers. Again the two methods are in excellent agreement and the above-mentioned trend portrays itself quite clearly.

To establish the validity of the combined convection–radiation heat transfer model a number of cases were compared to those presented by Tamehiro *et al.* [7] for the limiting case of no scattering. These verification runs, which were made over wide ranges of optical thickness, conduction–radiation parameters and mass-loading ratios, showed almost negligible differences between heat transfer predictions. The reason for such good comparison is largely attributed to the use of similar eddy diffusivity models in the laminar sublayers and turbulent core. Changing the eddy diffusivity in the sublayers to the one suggested by Deissler [13] resulted in an approximate difference of 10% compared with those presented by Tamehiro *et al.* [7]. Although the verification runs are not presented here one can still roughly compare results in Fig. 4 by simply multiplying their conduction–radiation parameters (N_R) by a factor of 8. (The factor of 8 is a direct result of basing the conduction–radiation parameter on the inlet temperature rather than the wall temperature as done by [7].

The total local Nusselt number Nu, mixed mean temperature θ_{mm}, and radiative heat flux ratio q^R/q^T (note that this ratio is analogous to the ratio of radiative to total Nusselt number) vs. axial distance $(x/R)/RePr$ are shown for various representative convective and radiative parameters in Figs. 2–18. In all the following results, assumptions (5), (6) and (7) have been invoked due to the lack of better knowledge,

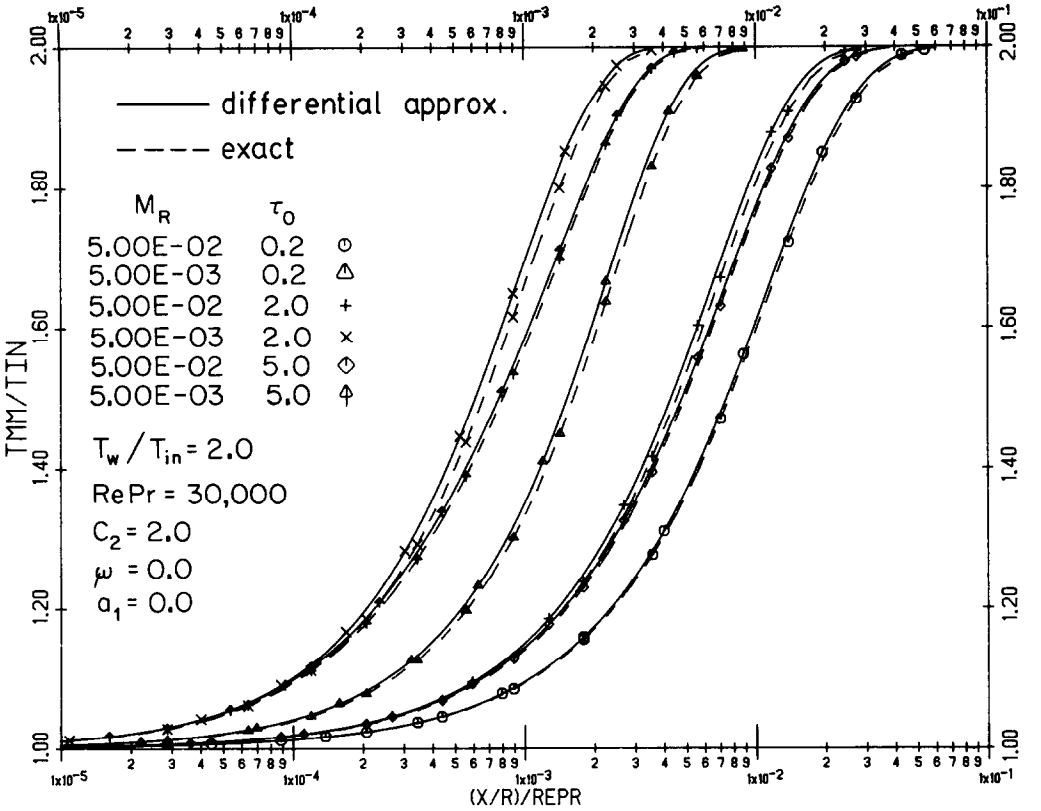

FIG. 2. Comparison between mixed-mean temperature development obtained from exact relations and the differential approximation.

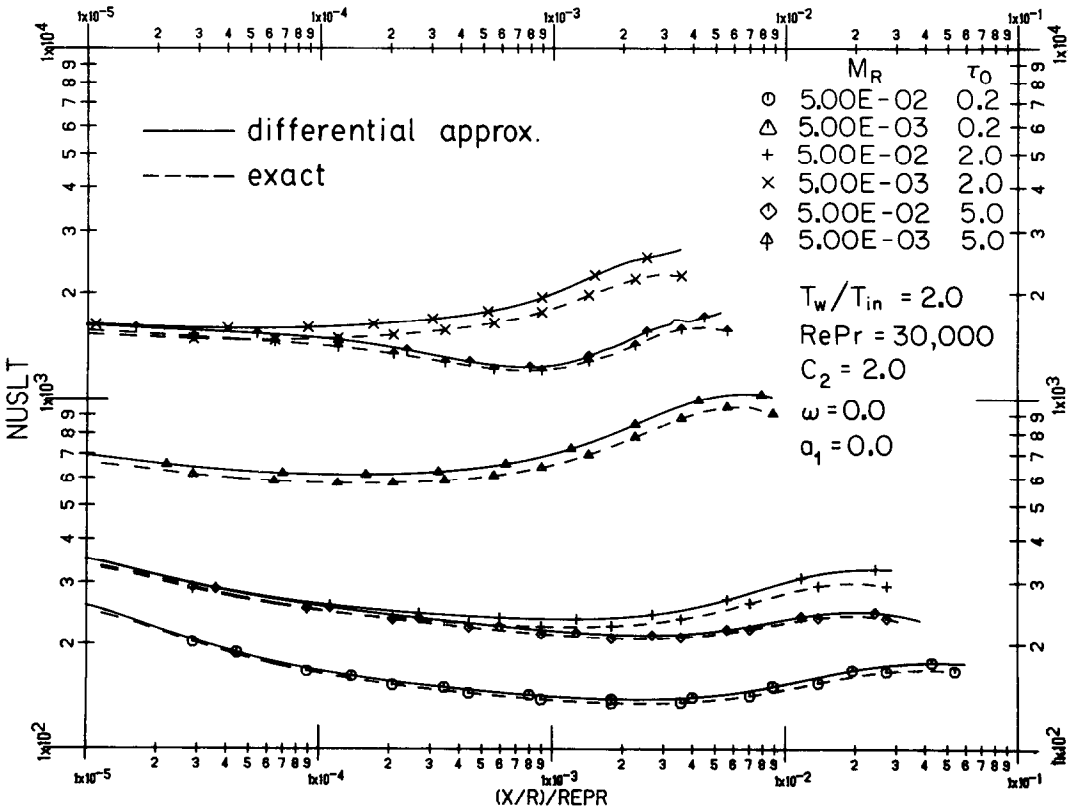

FIG. 3. Comparison between Nusselt number development obtained from exact relations and the differential approximation.

as well as assumption (1) and (3) in order to limit the scope of the results somewhat. Further, it is assumed that $C_1 \gg 1$. Nevertheless, the results presented here qualitatively cover an extremely large range of convection and radiation parameters which are condensed into the following four cases.

(1) The effect of the conduction–radiation parameter M_R and the optical thickness based on the absorption coefficient κR, are shown in Figs. 4–9 for Nu, θ_{mm} and q^R/q^T vs. axial distance, respectively; the first three pertain to the hot wall–cold medium case, while the other three show the trends for the cold wall–hot medium case.

(2) The qualitative influence of the single scattering albedo ω, and the degree of anisotropy a_1 on Nu, θ_{mm} and q^R/q^T variations, respectively, are shown in Figs. 10, 11, and 12.

(3) Case 3 represents the influence of the specific mass loading ratio C_2, and wall temperature T_w/T_i. The influence of these parameters on Nu, θ_{mm} and q^R/q^T are shown in Figs. 13, 14, and 15, respectively.

(4) Finally, the influence of the gas Reynolds number on Nu, θ_{mm} and q^R/q^T is shown in Figs. 16, 17, and 18, respectively.

Case 1. Figures 4, 5 and 6 demonstrate the influence of the conduction–radiation parameter M_R and optical thickness based on absorption κR, on the overall heat transfer rates in non-scattering turbulent suspension flows for the case of a heated wall. Due to the nonlinear radiative contribution no fully-developed temperature profile, and consequently no asymptotic Nusselt number, develops. Rather, for the heated-wall case, the Nusselt number goes through a minimum at a certain downstream location, behind which it tends to increase again. The location of the minimum moves towards the inlet with increasing importance of radiation. Radiation becomes more dominant with decreasing M_R due to the accompanying rise in temperature level with its increased radiative emission. The appearance of a minimum Nusselt number may be explained as follows: downstream from the inlet total flux as well as the relevant temperature difference, $T_w - T_{mm}$, decrease monotonically. However, while in the convection-only case q^T decreases always more rapidly than $T_w - T_{mm}$, this is not the case if strong radiation is present, as can be seen from the continuously increasing values for q^R/q^T (cf. Fig. 6).

In the optically-thin limit $\kappa R = 0$ (no absorption and emission takes place in the medium), as well as in the optically-thick limit $\kappa R \to \infty$ (radiation is absorbed directly at the point of emission), the radiative contribution must vanish. Thus, the Nusselt number must go through a maximum at a certain optical thickness as is clearly demonstrated in Fig. 4.

The behavior of mixed-mean temperature θ_{mm}, and relative radiative flux q^R/q^T corresponds to the Nusselt

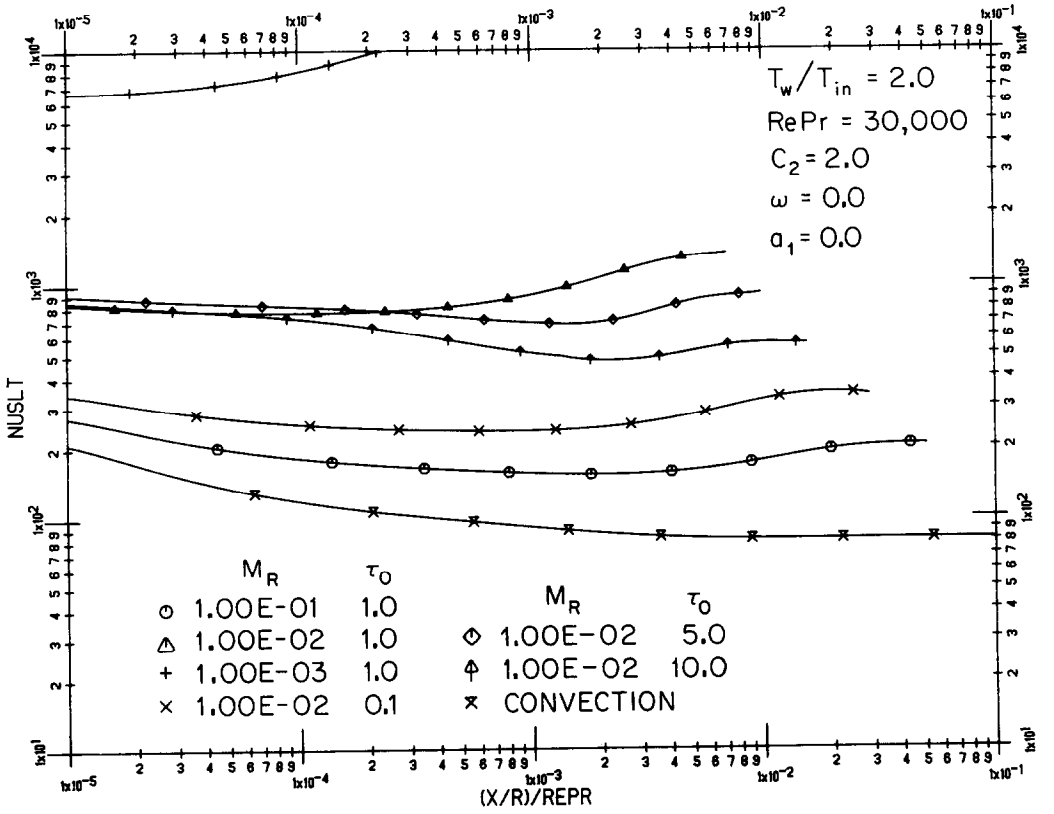

FIG. 4. Influence of optical thickness and conduction–convection parameter on Nusselt number development—heated wall.

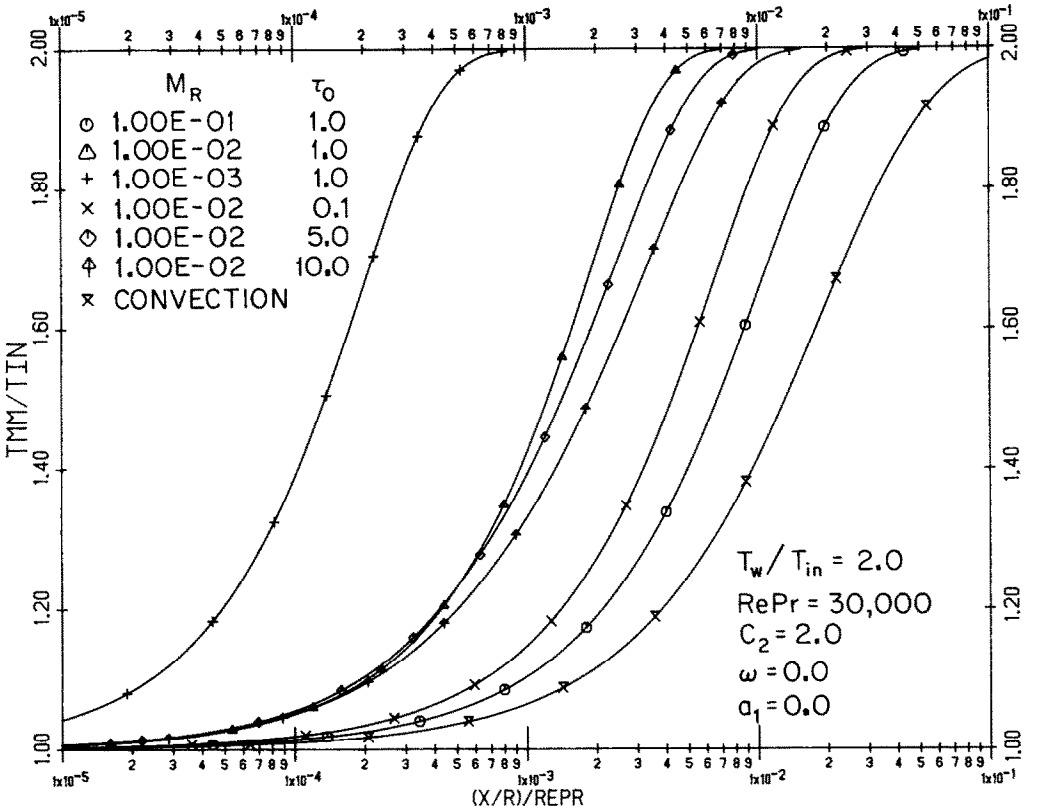

FIG. 5. Influence of optical thickness and conduction–convection parameter on mixed-mean temperature development—heated wall.

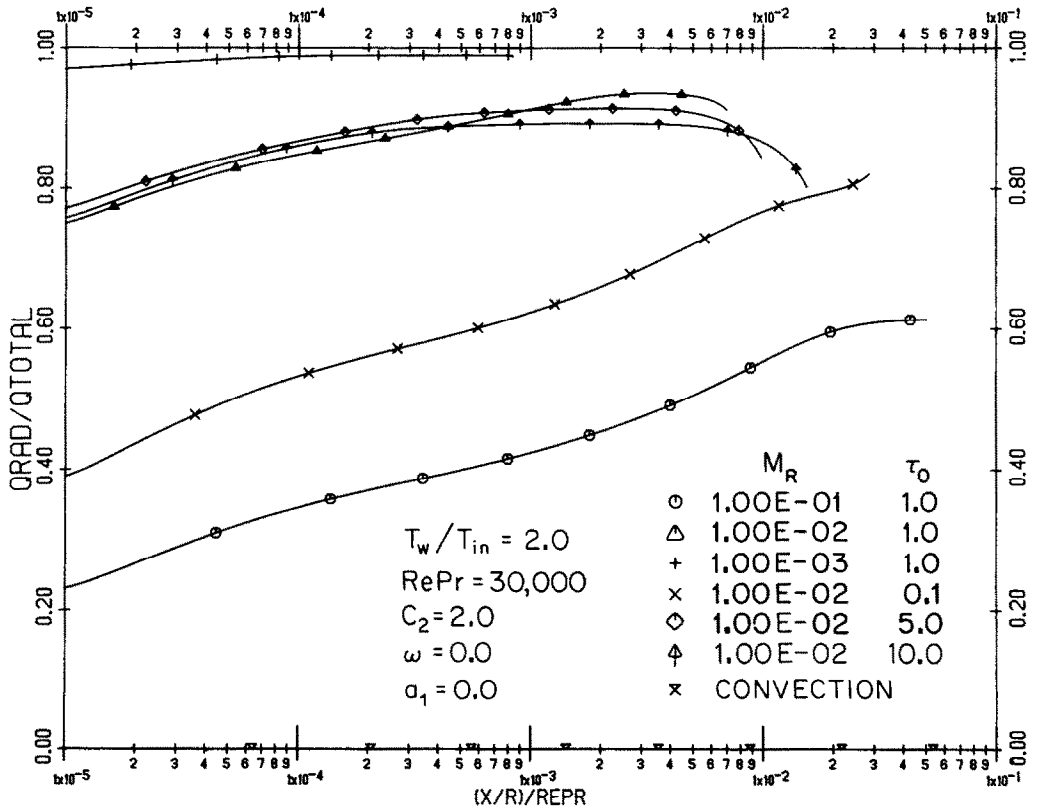

FIG. 6. Influence of optical thickness and conduction–convection parameter on relative radiative flux—heated wall.

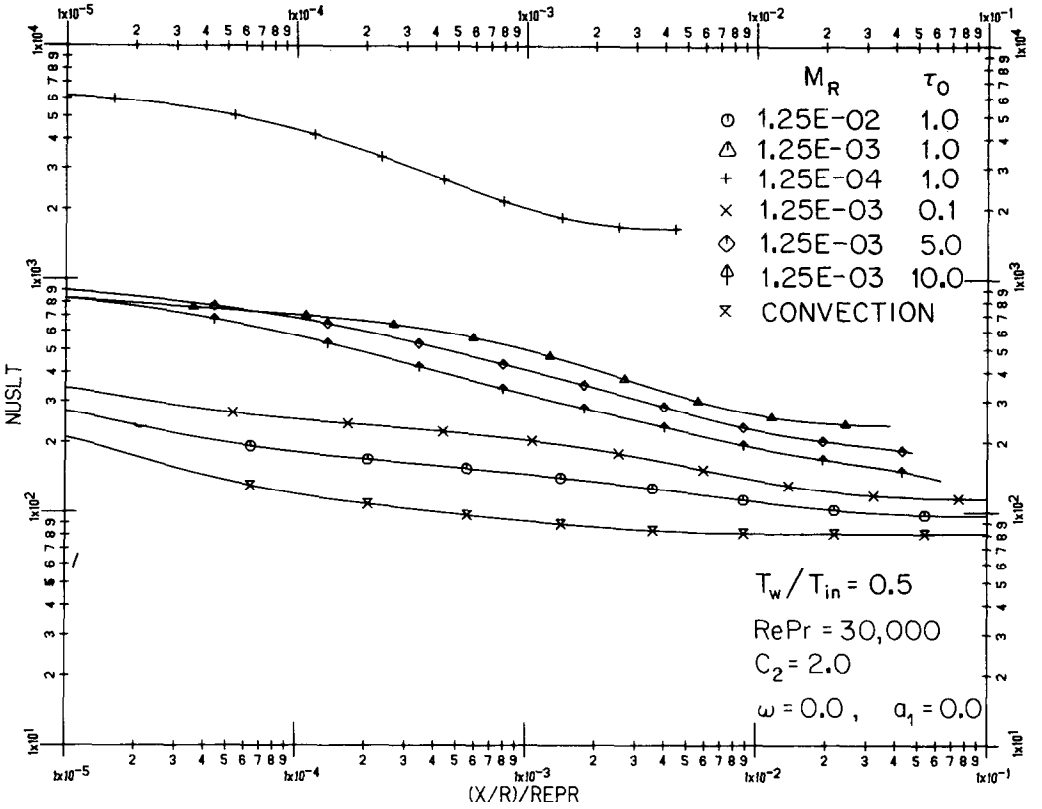

FIG. 7. Influence of optical thickness and conduction–convection parameter on Nusselt number development—cooled wall.

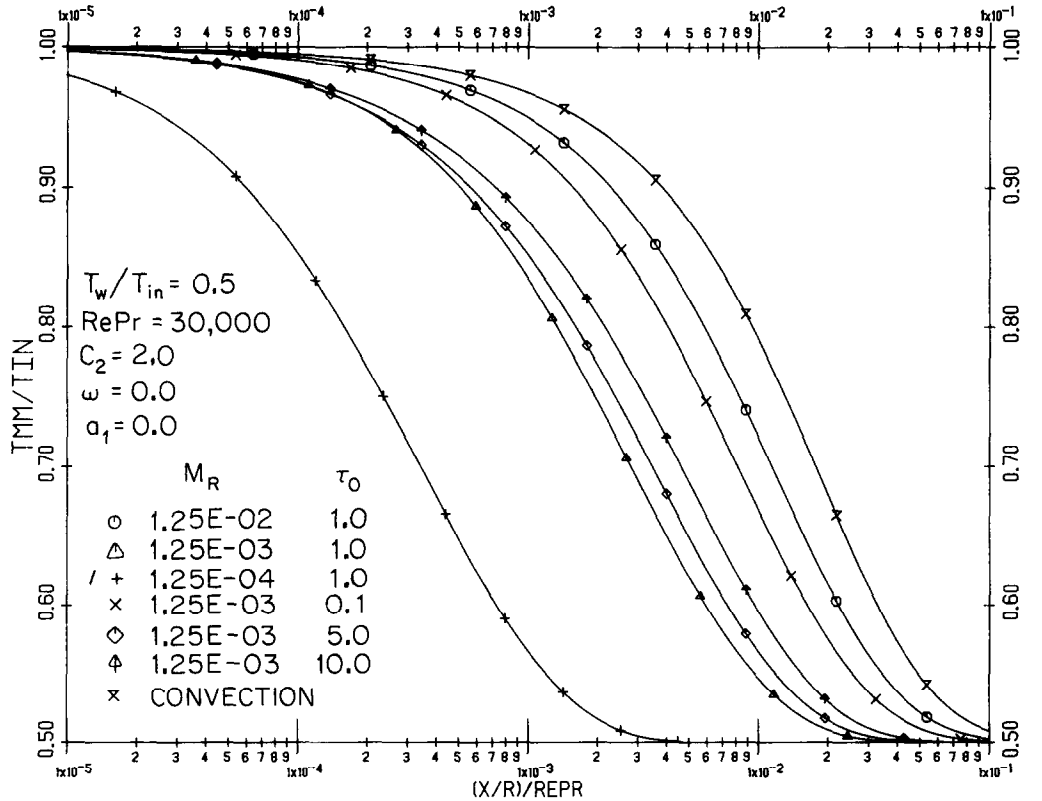

FIG. 8. Influence of optical thickness and conduction–convection parameter on mixed-mean temperature development—cooled wall.

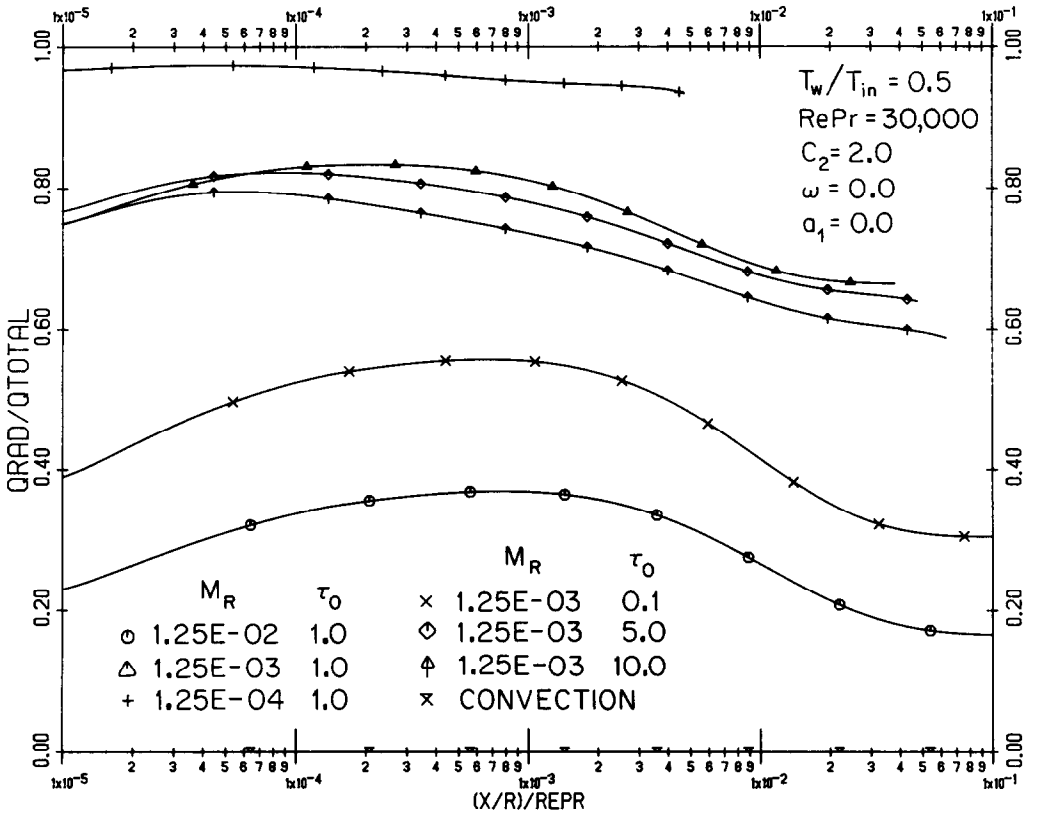

FIG. 9. Influence of optical thickness and conduction–convection parameter on relative radiative flux—cooled wall.

number behavior, i.e. the radiative flux increases with decreasing M_R, resulting in a more rapid change of θ_{mm}. Similarly, there exists an optimal optical thickness, resulting in a maximal radiative flux with corresponding maximal mixed-mean temperature build-up.

Figure 7 shows the Nusselt number curves for the corresponding hot medium–cold wall situation. In this case the fluid temperature drops as it moves along the tube and, therefore, the importance of radiation is reduced with axial distance. The presence of radiation still results in higher Nusselt numbers than the convection-only case. However, as opposed to the cold medium–hot wall situation, no relative minima in the Nusselt numbers are observed. Figure 8 depicts the corresponding mixed-mean temperature variations with axial position for the cold-wall case. The trends are similar to the previous one; i.e. higher levels of radiation result in more rapid development of the mixed-mean temperatures. Figure 9 demonstrates the behavior of radiative heat flux ratios for the hot medium–cold wall condition. These curves show that the relative radiative heat flux contribution increases to a maximum value at a certain axial position and decreases beyond that point. Also, it is observed that the maxima become more pronounced in cases with relatively lower radiation (small κR or large M_R). This behavior is due to the fact that in situations where only a small amount of radiation is present, the fluid core remains hot for a longer period of time while, at the same time, the layers of fluid closer to the tube wall are cooled by convection. Establishment of such a temperature gradient causes an increase in the radiative heat flux until a point where the core temperature starts dropping. The corresponding mixed-mean temperature variations show that, indeed, the maxima for the radiative heat flux profiles occur at the same axial position where the mixed-mean temperature curves start their rapid decline, indicating the cooling of the fluid core.

Case 2. It is seen that an increase in scattering (increasing ω) causes a decrease in radiative and, therefore, overall heat flux, even if absorption and emission are held constant (Fig. 12). This is due to the fact that, with increasing scattering, more and more radiation emitted in a hot region is scattered back towards the region of emission rather that travelling on towards colder parts. This increased resistance for transmission of radiation then causes a decrease in heat transfer (Fig. 10) and slows the development of the mixed-mean temperature (Fig. 11). As expected, the effect is particularly important in the case of strong backward scattering ($a_1 = -1$), especially for large scattering albedo. On the other hand, in the case of strong forward scattering ($a_1 = +1$) much of the scattered energy behaves similar to transmitting radiation, thus reducing the influence of scattering. It is interesting to note that the reduction in heat transfer rates is rather small for fairly large values of ω, say $\omega =$

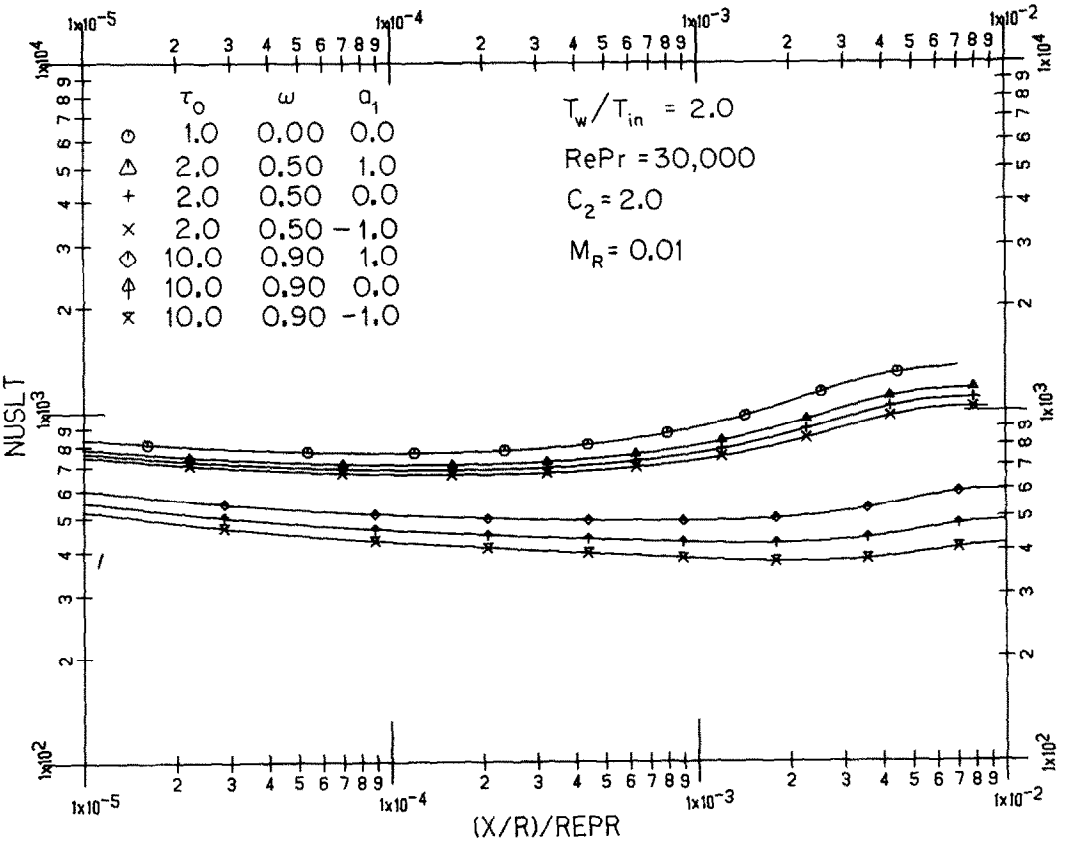

FIG. 10. Influence of scattering albedo and anisotropy on Nusselt number development.

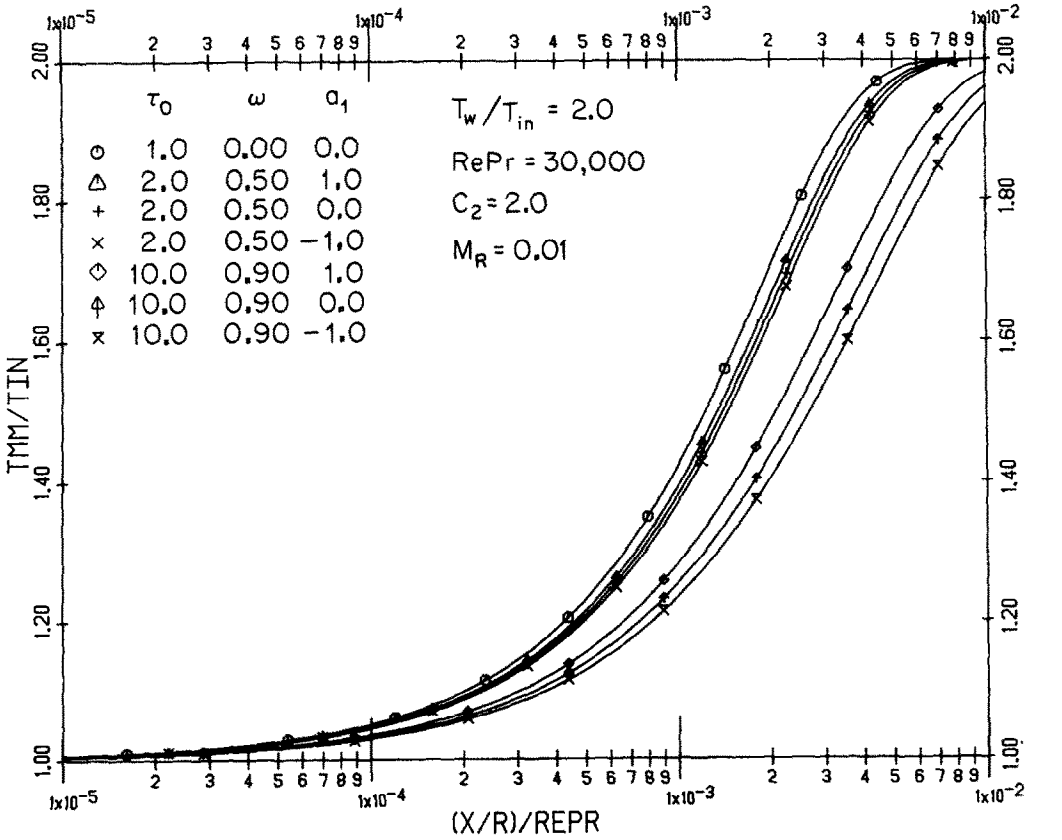

FIG. 11. Influence of scattering albedo and anisotropy on mixed-mean temperature development.

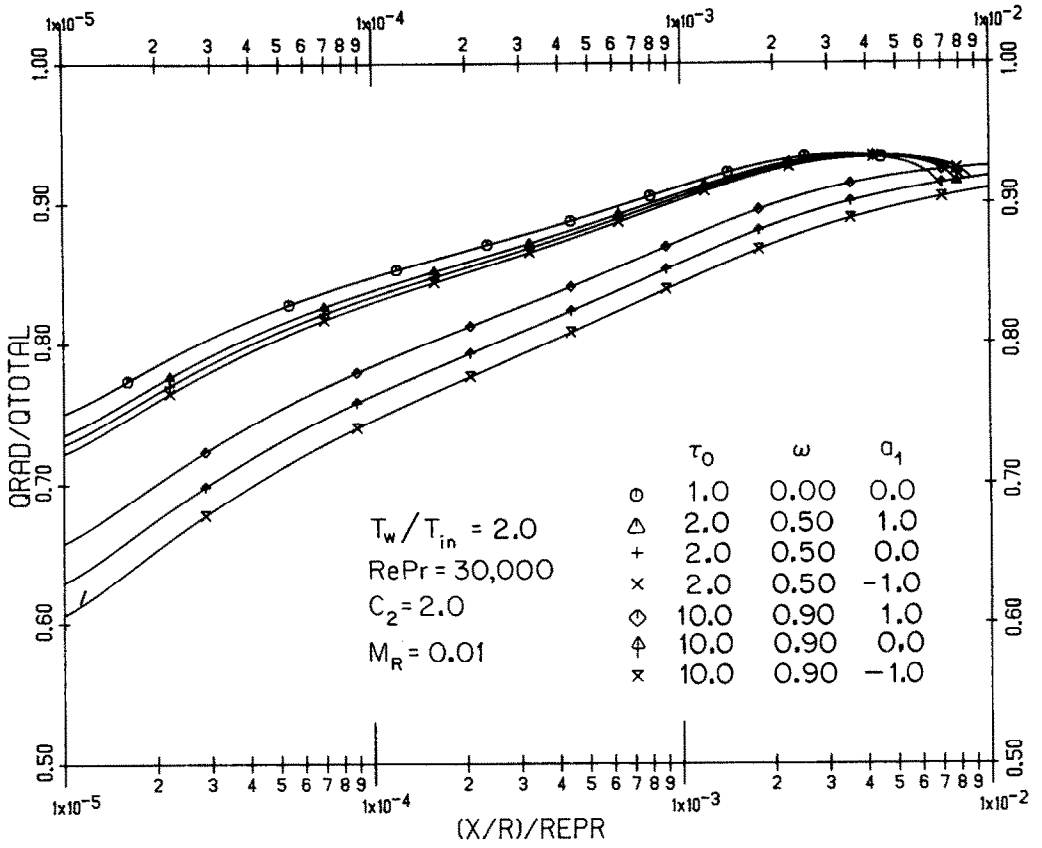

FIG. 12. Influence of scattering albedo and anistropy on relative radiative flux.

0.5, regardless of degree of anisotropy.

While the reduction of heat flux rates and Nusselt number is substantial for large values of ω (Fig. 10), overall heat transfer rates still remain an order of magnitude higher (for the present case) than for the convection-only case (cf. Fig. 4).

Case 3. Figures 13, 14 and 15 demonstrate the influence of wall temperature level T_w/T_i, and solid-to-gas mass loading ratio C_2 on heat transfer rates. This is shown for constant and moderate values of the conduction-to-radiation parameter M_R (based on inlet temperature), and optical thickness κR for a non-scattering medium. It is seen that, for increasing C_2, the curves for Nu and θ_{mm} are basically just stretched by a factor of $(1+C_2)$ in the axial direction. This will, obviously, always be the case as long as $\theta_p \simeq \theta_f$, as can be seen by adding equations (1), and (2). It should be borne in mind, however, that an increase in mass loading ratio C_2 will usually be accompanied by a similar increase in absorption coefficient κ.

As expected, the level of tube wall temperature influences heat transfer rates profoundly: if the wall temperature is doubled, near the inlet the radiative flux increases to roughly 16-fold while the convective rate approximately doubles. This is shown in Fig. 15. At high temperatures radiation may be so strong that the Nusselt number starts to increase after only a minute fraction of a diameter downstream from the inlet (Fig. 13).

Case 4. To show the influence of Reynolds number on heat transfer rates the same basic radiation and suspension parameters M_R, C_2 and ω as in Case 3 were chosen. As is seen from Figs. 16 and 17, the influence of Reynolds number is much less pronounced. As expected, heat transfer rates and mixed-mean temperature development are increased with increasing Reynolds number as a direct result of the increased eddy diffusivity. For comparison, a laminar case with identically-zero eddy diffusivity is also included. The increased convection is further demonstrated in Fig. 18. While convection is increased, radiative fluxes are decreased somewhat due to the faster developing temperature profile, resulting in significantly lower values for q^R/q^T.

CONCLUSIONS

The interaction between radiation and laminar or turbulent forced convective heat transfer in a gas–particulate suspension flow through a circular tube and the effects of various radiation and convection parameters on Nusselt numbers, mixed-mean temperature, and relative magnitude of radiative flux have been discussed in some detail. The results ob-

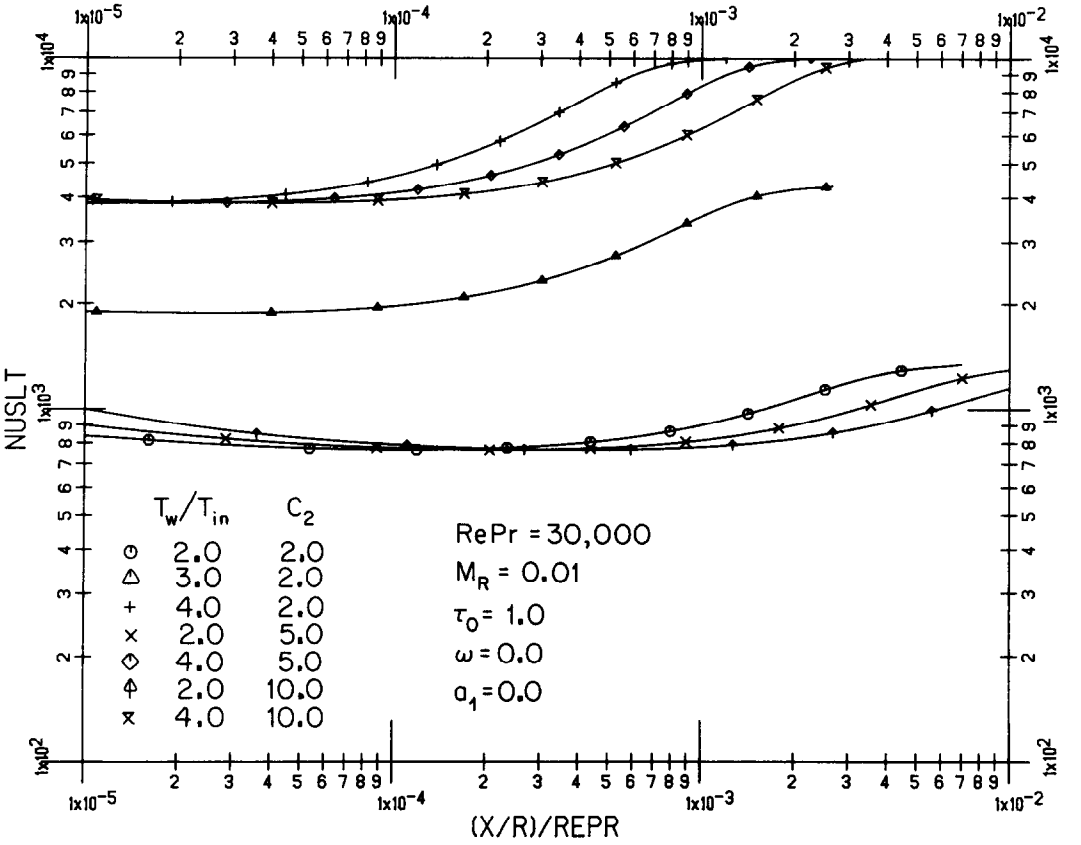

FIG. 13. Influence of temperature level and mass loading ratio on Nusselt number development.

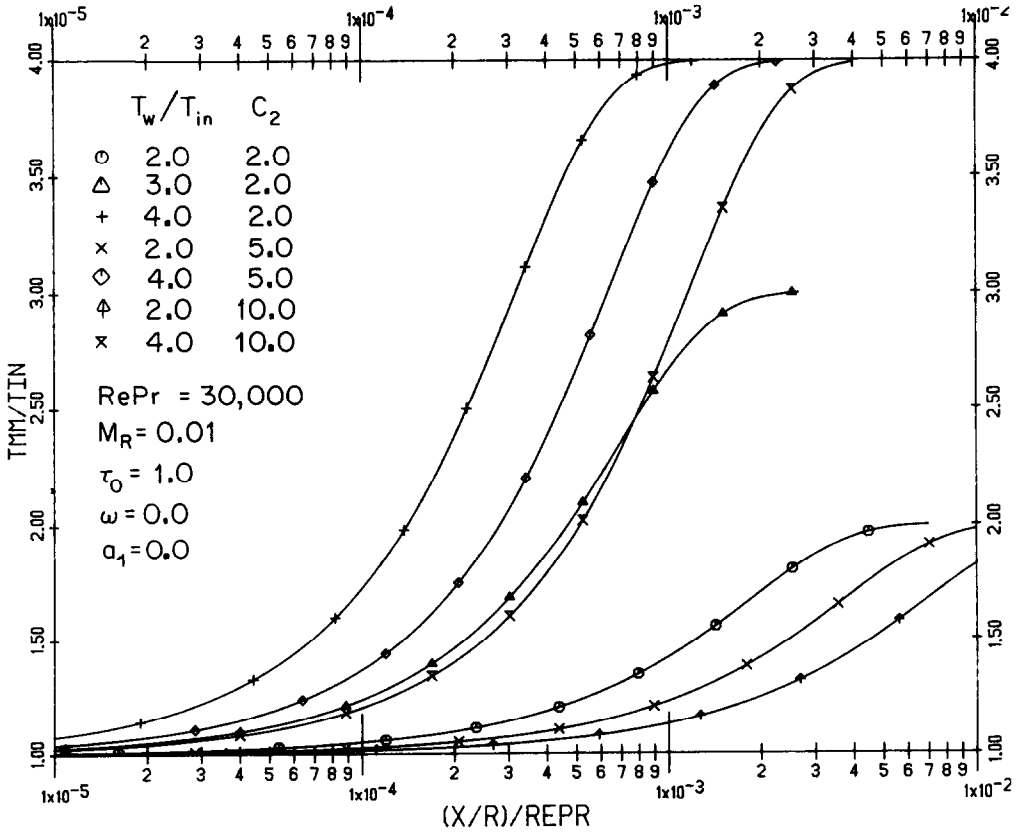

FIG. 14. Influence of temperature level and mass loading ratio on mixed-mean temperature development.

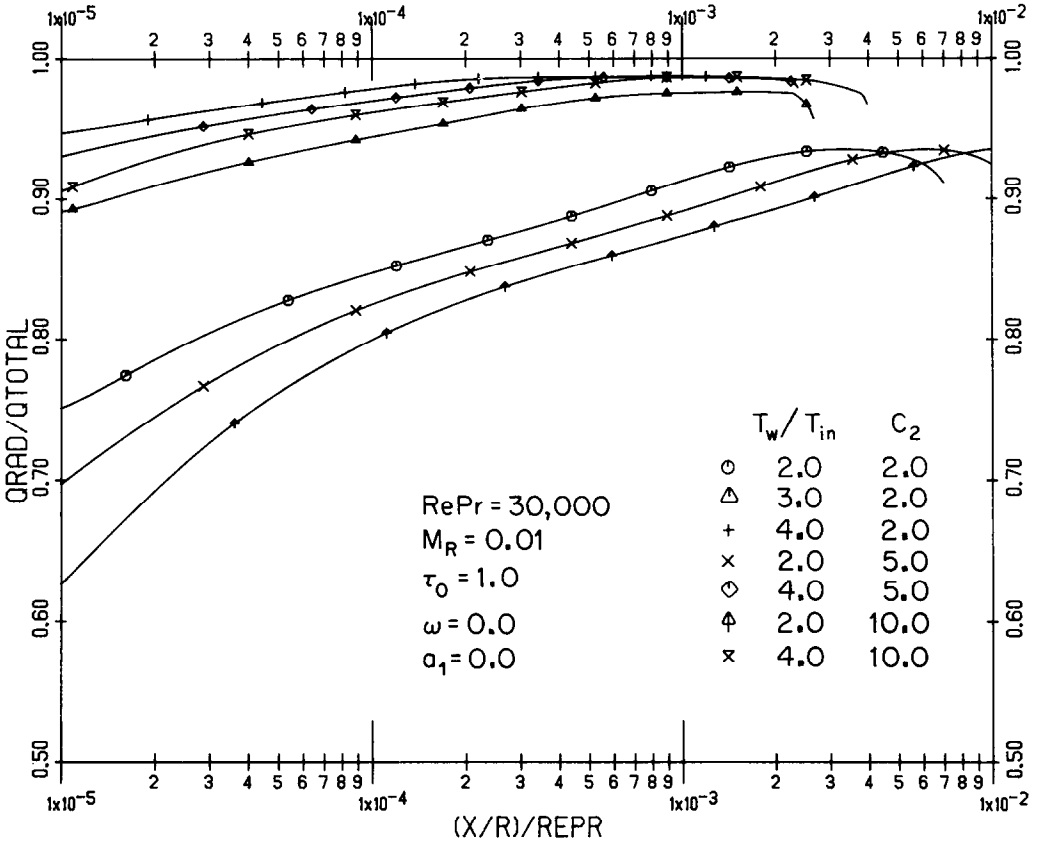

FIG. 15. Influence of temperature level and mass loading ratio on relative radiative flux.

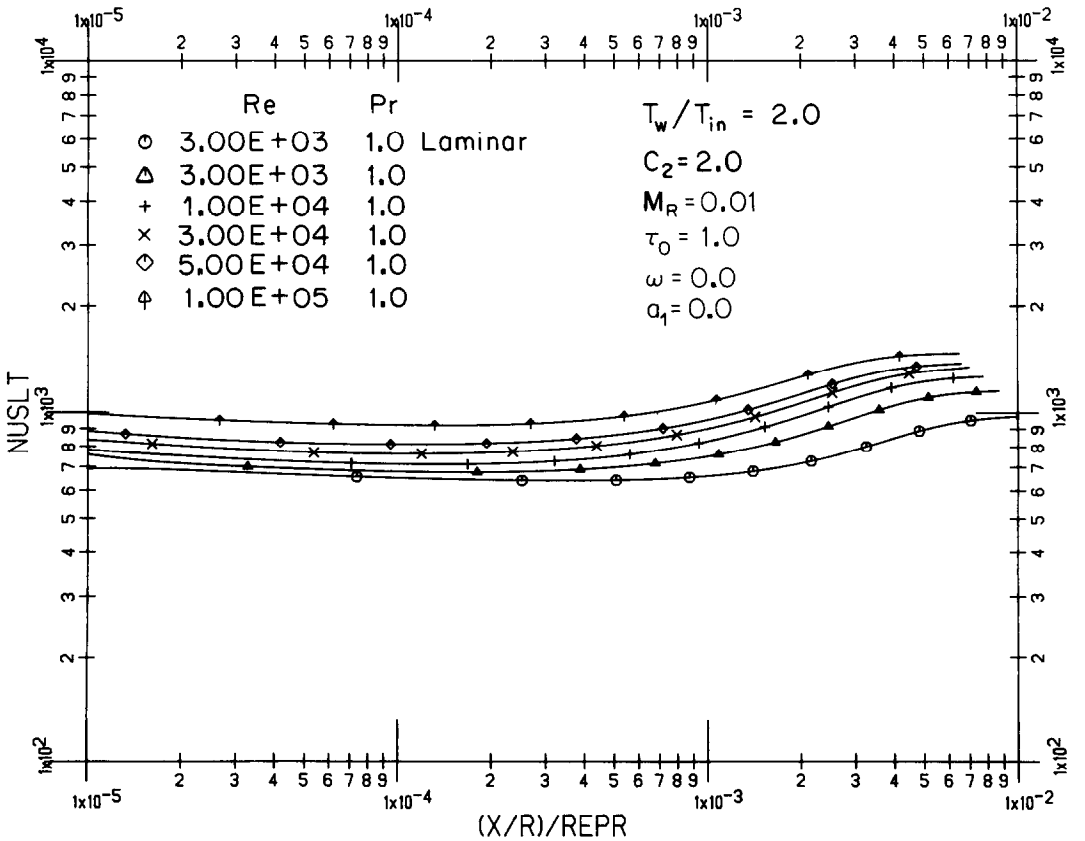

FIG. 16. Influence of Reynolds number on Nusselt number development.

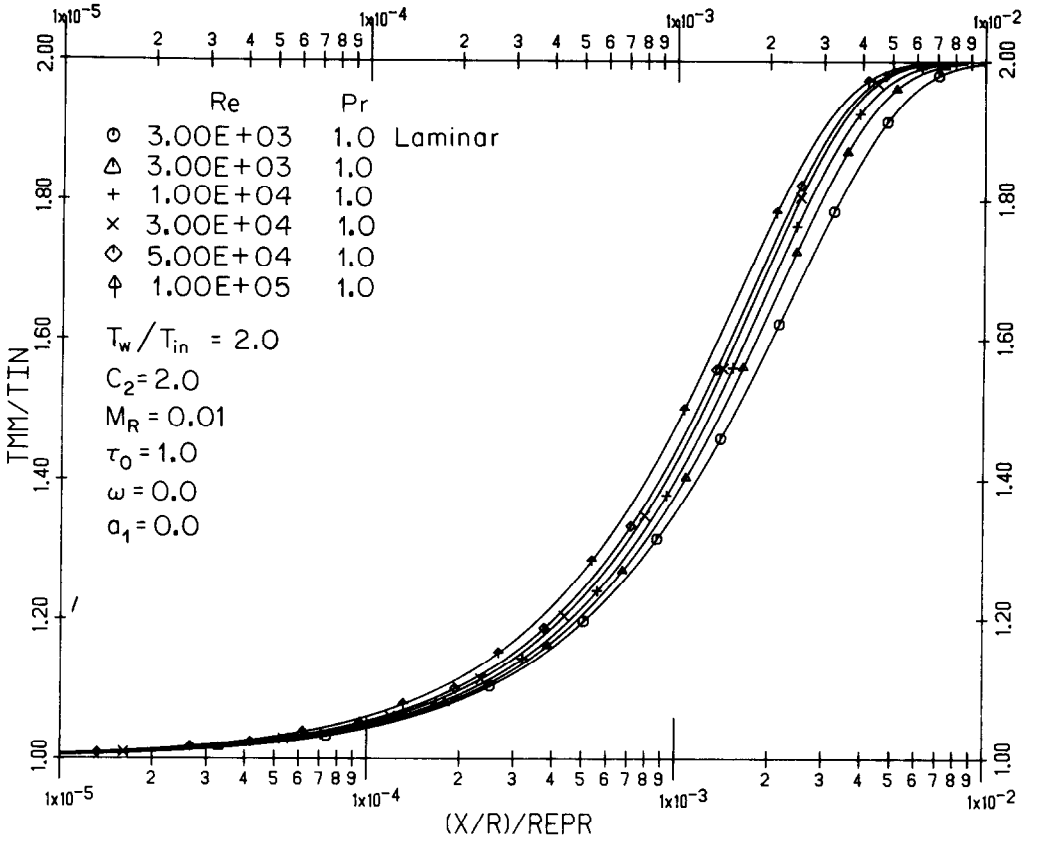

FIG. 17. Influence of Reynolds number on mixed-mean temperature.

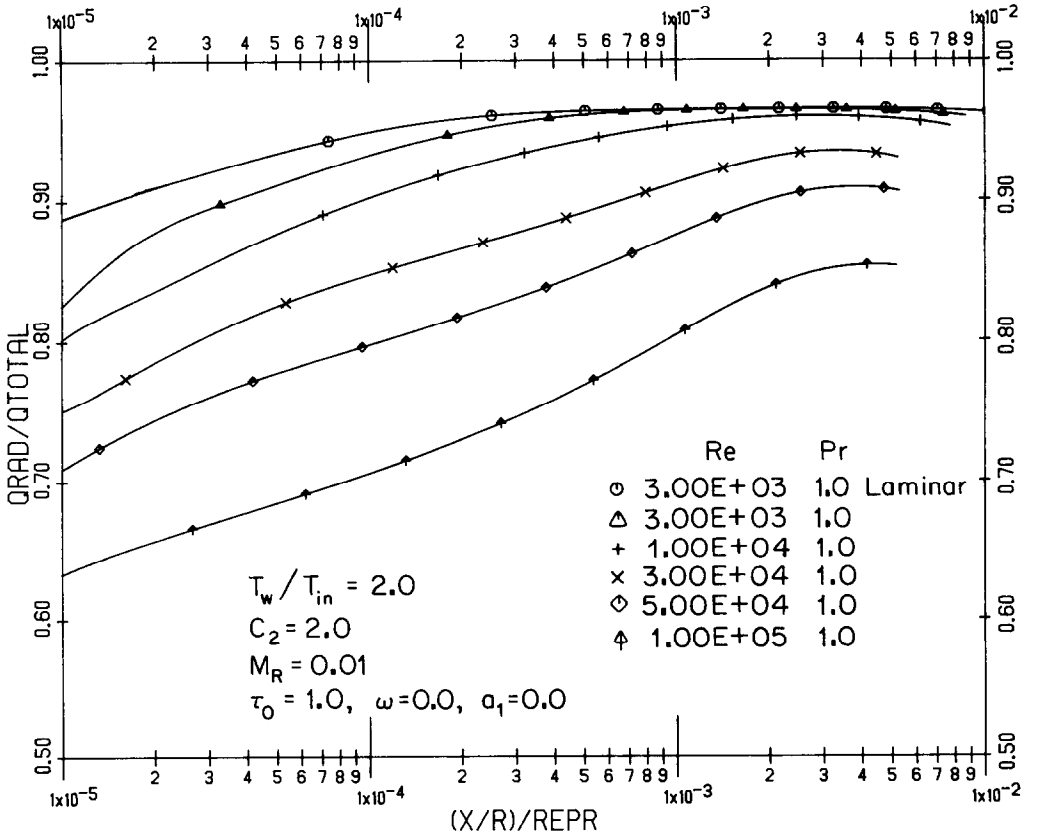

FIG. 18. Influence of Reynolds number on relative radiative flux.

tained may be summarized as follows:

(1) For the case of $T_w/T_i > 1$, if radiation effects must be included, no fully-developed temperature profile can be expected to form. Generally, the Nusselt number tends to go through a minimum at a certain downstream location, behind which it tends to increase. For strong radiation this minimum may be extremely close to the inlet. Of course, far downstream when $\theta_{mm} \to \theta_w$ one may linearize the radiation contribution resulting in fully developed profiles. However, this is of little practical importance since the Nusselt number varies drastically over the region of maximum mixed-mean temperature change. This is quite unlike the convection-only case where the largest portion of the mixed-mean temperature change occurs essentially at the asymptotic Nusselt number. By examining Figs. 4 and 5 it is evident that for the convection-only case approx. 95% of the mixed-mean temperature change occurs at the asymptotic Nusselt number whereas for cases with radiatively participating particulates the Nusselt number increases markedly over the region of the steepest mixed-mean temperature gradient and is still increasing at $\theta_w - \theta_{mm} = 0.01$. Hence the asymptotic value for the Nusselt number becomes of less importance with increased radiative contribution.

Even in the cold-wall case, $T_w/T < 1$, where an asymptotic Nusselt number does establish itself, this asymptotic value is of relatively small importance as it also is established too far downstream (Figs. 7 and 8).

(2) While the differential approximation consistently overpredicts radiative wall fluxes slightly, these errors do not accumulate downstream. Thus, this approximation may be used with good accuracy under all optical conditions.

(3) For every flow situation there exists an optimum solid-loading ratio for which maximum heat transfer rates are achieved: while adding solids to the flow increases the thermal entry it also increases the optical thickness of the mixture, resulting in maximum radiative heat transfer rates at some intermediate optical thickness.

(4) Radiative scattering tends to decrease heat transfer rates even if emission and absorption remain unaffected. However, scattering is unimportant for up to relatively large values of the single scattering albedo. Effects of anistropic scattering are important only for very large values of the single scattering albedo.

(5) Even with particle radiation present, the solid-to-gas mass loading ratio simply tends to stretch the thermal entry. Thus, if the particles are sufficiently small, and in the absence of chemical reactions, particle and fluid temperature remain essentially the same. Consequently, one could combine the two energy equations to form a single continuum.

(6) In turbulent flow the radiative heat transfer does change with Reynolds number and is, therefore, not independent of the flow field. The fraction of convective as compared to total heat transfer rate increases with increasing Reynolds number as a result of the increased eddy turbulence.

Acknowledgement—The support of the National Science Foundation under Grant ENG 77-12628 is gratefully acknowledged.

REFERENCES

1. L. Farbar and M. J. Morley, Heat Transfer to Flowing Gas–Solids Mixtures in a Circular Tube, *Ind. Engng Chem.* **49**, 1143–1150 (1957).
2. C. L. Tien, Heat Transfer by Turbulently Flowing Fluids–Solids Mixtures in a Pipe, *Trans. ASME, J. of Heat Transfer* **C83**, 183–188 (1961).
3. L. Farbar and C. A. Depew, Heat Transfer Effects to Gas–Solids Mixtures Using Solid Spherical Particles of Uniform Size, *Ind. Engng Chem. Fundam.* **2**, 130–135 (1963).
4. C. A. Depew and L. Farbar, Heat Transfer to Pneumatically Conveyed Glass Particles of Fixed Size, *Trans. ASME, J. of Heat Transfer.* **C85**, 164–172 (1963).
5. R. Echigo and S. Hasegawa, Radiative Heat Transfer by Flowing Multiphase Medium—Part I. An Analysis on Heat Transfer of Laminar Flow Between Parallel Flat Plates, *Int. J. Heat Mass Transfer* **15**, 2519–2534 (1972).
6. R. Echigo, S. Hasegawa and H. Tamehiro, Radiative Heat Transfer by Flowing Multiphase Medium—Part II. An Analysis on Heat Transfer of Laminar Flow in an Entrance Region of Circular Tube, *Int. J. Heat Mass Transfer* **15**, 2595–2610 (1972).
7. H. Tamehiro, R. Echigo and S. Hasegawa, Radiative Heat Transfer by Flowing Multiphase Medium—Part III. An Analysis on Heat Transfer of Turbulent Flow in a Circular Tube, *Int. J. Heat Mass Transfer* **16**, 1199–1213 (1973).
8. T. C. Chawla and S. H. Chan, Combined Radiation and Convection in Thermally Developing Poiseuille Flow with Scattering, *Trans. ASME, J. of Heat Transfer* **C102**, 297–302 (1980).
9. S. deSoto, Coupled Radiation, Conduction and Convection in Entrance Region Flow, *Int. J. Heat Mass Transfer* **11**, 39–53 (1968).
10. F. H. Azad and M. F. Modest, Evaluation of the Radiative Heat Flux in Absorbing, Emitting and Linear-Anisotropically Scattering Cylindrical Media, *Trans. ASME, J. of Heat Transfer* **C103**, 350–356 (1981).
11. M. F. Modest and F. H. Azad, The Differential Approximation for Radiative Transfer in an Emitting, Absorbing and Anisotropically Scattering Medium, *J. quant. Spectrosc. Radiat. Transfer* **23**, 117–120 (1980).
12. M. F. Modest and F. H. Azad, The Influence and Treatment of Mie-Anisotropic Scattering in Radiative Heat Transfer, *Trans. ASME, J. of Heat Transfer* **C102**, 92–98 (1980).
13. W. M. Kays, Convective Heat and Mass Transfer, McGraw-Hill, (1966).
14. H. Reichardt and Z. Angew, *Math. Mech.* **31**, 208 (1951).
15. D. Spalding, *Conf. Intern. Developments in Heat Transfer, ASME, Boulder, Colorado, Part II*, 439–446 (1961).
16. A. T. Wassel and D. K. Edwards, Molecular Gas Radiation in a Laminar or Turbulent Pipe Flow, *Trans. ASME, J. of Heat Transfer* **C98**, 101–107 (1976).

COUPLAGE DE RAYONNEMENT ET DE CONVECTION DANS L'ECOULEMENT EN CONDUITE D'UN GAZ ABSORBANT, EMISSIF ET ANISOTROPIQUEMENT DIFFUSANT

Résumé—On développe une procédure numérique pour étudier l'interaction du rayonnement thermique, de la conduction et de la convection dans un écoulement d'une suspension dans un gaz à l'intérieur d'un tube à section circulaire. Une analyse est conduite sur l'écoulement turbulent d'un milieu multiphasique avec des particules qui absorbent, émettent et diffusent de façon anisotrope, les parois étant chauffées ou refroidies à température constante. La contribution du rayonnement thermique est obtenue en modifiant l'approximation différentielle pour une diffusion anisotrope linéaire qui est montrée être précise par comparaison avec quelques solutions exactes. Les équations différentielles sont trois équations (non-linéaires) couplées qui sont résolues numériquement par une méthode implicite aux différences finies avec une procédure itérative. Les résultats sont résumés pour de larges domaines des paramètres.

STRAHLUNG UND KONVEKTION IN ABSORBIERENDER, EMITTIERENDER UND ANISOTROP STREUENDER STAUB–GAS-ROHRSTRÖMUNG

Zusammenfassung—Ein numerisches Verfahren zur Untersuchung der Wechselwirkung zwischen thermischer Strahlung sowie Wärmeleitung und Konvektion in einer sich thermisch ausbildenden Staub–Gas-Strömung in einem Kreisrohr wurde entwickelt. In der vorliegenden Studie wird eine Analyse der turbulenten Strömung eines mehrphasigen Mediums mit absorbierenden, emittierenden und anisotrop streuenden Teilchen durchgeführt, wobei die Strömung won einer Wand konstanter Temperatur beheizt oder gekühlt wird. Der Beitrag der thermischen Strahlung wird durch Modifikation der differentiellen Näherung entsprechend der linear anisotropen Streuung erhalten, die sich im Vergleich mit einigen exakten Lösungen als genau erweist. Die maßgebenden Differentialgleichungen werden als drei gekoppelte (nichtlineare) Gleichungen hergeleitet, die durch ein implizites finites Differenzen-Verfahren mit iterativer Verarbeitung der einzelnen Terme für die Staubteilchen numerisch gelöst werden. Die Ergebnisse sind für große Parameterbereiche zusammengefaßt.

ВЗАИМОСВЯЗАННЫЙ ЛУЧИСТЫЙ И КОНВЕКТИВНЫЙ ТЕПЛОПЕРЕНОС ПРИ ТЕЧЕНИИ В ТРУБЕ ПОГЛОЩАЮЩИХ, ИЗЛУЧАЮЩИХ И АНИЗОТРОПНО РАССЕИВАЮЩИХ СИСТЕМ «ГАЗ–ТВЕРДЫЕ ЧАСТИЦЫ»

Аннотация — Предложен численный метод исследования взаимодействия теплового излучения с теплопроводностью и конвекцией при термически развитом течении в круглой трубе взвешенных в газе твердых частиц. Выполнен анализ турбулентного течения многофазной среды с поглощающими, излучающими и анизотропно рассеивающими твердыми частицами в канале, ограниченном нагретыми или охлажденными стенками постоянной температуры. С помощью модифицированного дифференциального приближения, в котором учитывается линейно анизотропнос рассеивание, проведен расчет теплового излучения, достоверность результатов которого проверена сопоставлением с некоторыми точными решениями. Выведены основные дифференциальные уравнения в виде трех взаимосвязанных (нелинейных) соотношений, которые решены численно неявным итерационным методом конечных разностей. Результаты обобщены на широкие диапазоны параметров.